International Journal of Thermofluids 23 (2024) 100742

Contents lists available at ScienceDirect

International Journal of Thermofluids

journal homepage: www.sciencedirect.com/journal/international-journal-of-thermofluids

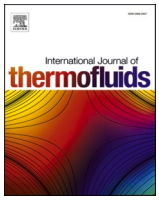

Experimental isochoric apparatus for bubble points determination: Application to CO_2 binary mixtures as advanced working fluids

M. Doninelli *, G. Di Marcoberardino, C. M. Invernizzi, P. Iora

Università degli Studi di Brescia, Dipartimento di Ingegneria Meccanica ed Industriale, via Branze, 38, 25123, Brescia, Italy

ARTICLE INFO

Keywords:
CO_2 mixtures
Vapour–liquid equilibrium
Bubble points
Transcritical cycles
Experimental campaign

ABSTRACT

Carbon dioxide binary mixtures are increasingly considered as working fluids in transcritical power cycles, due to the capability to perform liquid-phase compression even at high environmental temperatures. However, a robust thermodynamic model is essential for optimal and reliable design conditions. It is widely recognised that fine-tuning the equation of state with experimental vapour-liquid equilibrium data of the mixture significantly enhances its reliability.

In this work, a new apparatus dedicated to vapour-liquid equilibrium measurements of mixtures is presented. The proposed method consists of a constant-volume system, where bubble points are identified from the divergence of slope of the isochoric lines between the two-phase and liquid regions, in the temperature-pressure plane. The temperature and pressure limits of the apparatus are 503 K and 25 MPa.

Bubble points of CO_2 binary mixtures with hexafluorobenzene (C_6F_6) and n-pentane (C_5H_{12}) have been measured and compared with previous literature data for validation purposes. Then, the CO_2 mixture with octafluorocyclobutane (c-C_4F_8) is experimentally studied, addressing a literature gap in bubble point data. The data are used to calibrate the thermodynamic model, leading to affordable design conditions of the power cycle compared to the non-optimised thermodynamics scenario, in a concentrated solar power tower plant.

1. Introduction

Starting from the theoretical conceptualisation of supercritical carbon dioxide (sCO_2) power cycles, attributed to Angelino [1] and Feher [2], nowadays there is a renewed and growing interest in this technology to replace the state-of-the-art steam Rankine cycle in different sectors. In particular, sCO_2 as working fluid is attractive in high-temperature applications such as nuclear [3], solar [4], and high-temperature waste heat [5], due to high thermal efficiency and power density. However, in hot environments, where ambient air easily approaches 308 K, such as in typical locations of concentrated solar power (CSP) plants the minimum cycle temperature in dry-cooling conditions is constrained at values around 323 K. As a result, the compressibility of pure sCO_2 at the compressor intake is penalised by the compression step, that is far from the critical point. For this reason, the H2020 Scarabeus [6] and H2020 Desolination [7] projects proposed the adoption of innovative working fluids constituted by binary mixtures where the CO_2 is blended with dopants having higher critical temperature [8]. In this way the critical temperature of the CO_2 binary mixture can reach higher values compared to pure CO_2 by acting on the mixture composition, thus it is possible to fully condense the working fluid even at high values of minimum cycle temperature. As investigated by Imre and Ahmed [9], the critical temperature has a strong effect on the performance of Rankine cycles. The primary effect is the opportunity to employ liquid-phase compression, bringing two main advantages: lower energy consumption for the compression step, and a less challenging pump design [10] compared to a sCO_2 compressor operating near critical conditions. Secondly, as a result of mixing CO_2 with a more complex dopant, the heat capacities within the recuperator are more balanced than pure sCO_2, reducing the layout complexity from a recompressed cycle to a simple recuperative cycle. The utilisation of CO_2 mixtures for efficiency improvement is also discussed in the review work of Chowdhury and Eshan [11]. Turja et al. [12] considered the use of a bottoming Organic Rankine Cycle to recover the rejected heat of a sCO_2 cycle, showing that at increasing main compressor temperature the sCO_2 is largely penalised (lower compressibility) while increases the production of the bottoming ORC. The use of CO_2-mixtures as working fluids in that context would penalise less the power production as the compression step can be in liquid phase even at high values of minimum cycle temperature.

The proposed CO_2 blended solution, in fact, results in efficiency gains especially at minimum cycle temperatures as high as 323 K, compared to

* Corresponding author.
E-mail address: m.doninelli002@unibs.it (M. Doninelli).

https://doi.org/10.1016/j.ijft.2024.100742

Available online 20 June 2024

Nomenclature

Acronyms

A	Heat Transfer Area
AAD	Average Absolute Deviation
AC	Air Cooled
CSP	Concentrated solar power
EoS	Equation of state
HTF	Heat transfer fluid
PHE	Primary Heat Exchanger
PR	Peng Robinson
REFPROP	Reference Fluid Thermodynamic and Transport Properties
RC	Recompressed
SR	Simple Recupered
TIT	Turbine Inlet Temperature, K
U	Overall Heat Transfer Coefficient
VLE	Vapour Liquid Equilibrium

Symbols

c	Cyclic
$\dot{m}$	Mass flow rate, kg s^{-1}
P	Pressure, MPa
Q	Thermal duty, MW
R	Universal Gas Constant
s	Entropy, kJ kg^{-1} K^{-1}
T	Temperature, K
W	Mechanical power, MW
x	Molar fraction, -

Greek symbols

η_{th}	Cycle Thermal Efficiency, -
ρ	Density, kg m^{-1}
ω	Pitzer acentric factor, -

Subscripts

cr	Critical
in	Inlet
min	Minimum
max	Maximum

using pure sCO_2 [13]. It is worth it to mention that CO_2-based mixtures have been considered as working fluid not only for power generation purposes but also in refrigeration systems and heat pumps [14,15] and cogeneration [16].

In general, the accurate knowledge of the phase boundaries of mixtures is crucial for the design and optimisation of closed thermodynamic cycles working in direct or inverse Rankine cycles. The evaluation of the power cycle efficiency and reliable design conditions strongly depend on the accuracy of the equation of state (EoS) used to determine the thermodynamic properties of the mixture and its phase behaviour. It is well known that, in case of mixtures, the reliability of the EoS is improved when the binary interaction parameters of the EoS are regressed based on experimental vapour-liquid equilibrium (VLE) data. When these adjustable parameters are tuned on experimental VLE data, the phase boundaries of the mixture are better represented by the EoS, which is crucial from the power cycle point of view. Chen [17] utilised experimental VLE data of CO_2 mixtures as input for a prediction model. This model correlates the binary interaction parameter of the Peng Robinson (PR) EoS - with van der Waals mixing rules - to the critical parameters and acentric factor of organic compounds in mixture with CO_2. In a similar way, Abdel-Azim [18] used experimental bubble points to train an artificial neural network model capable to predict the bubble pressure of oils.

Generally, VLE data of mixtures are measured with conventional Pressure-Volume-Temperature (PVT) systems and VLE apparatus. In PVT systems, the mixture is transferred into a cell, whose volume is varied with an automated piston under isothermal conditions, and the bubble point is determined from the divergence of the volumetric behaviour in the liquid phase and the two-phase field. A PVT cell has been recently utilised by the authors [19], in the context of H2020 Desolination project, to measure bubble points of a CO_2 mixture with $SiCl_4$ for high-temperature Rankine cycle application. Moreover, in the same work, a non-conventional approach has been adopted to measure additional bubble points with a vibrating tube densimeter. In VLE cells, instead, a small sample of fluid, from both liquid and vapour phases, is extracted, vapourised, and analysed with gas chromatography. To avoid dead volumes and large pressure drop within the cell, the adoption of a capillary rapid on-line sampling injector (ROLSI®) [20] become a practical standard for VLE cells. A VLE apparatus used for the measurement of CO_2 binary mixtures is well described in the experimental works of Coquelet and Valtz [21–23],. The same concept has been applied by Wu et al. [24] to measure VLE data of CO_2+fluoroethane (R161) binary system. A VLE apparatus with ROLSI has been also used by Sadaghiani et al. [25] to measure a CO_2 binary mixture with 3,3, 3-Trifluoropropene and, subsequently, tune the binary interaction parameters of different EoS.In the context of the project, the CO_2 mixture with C_6F_6 has been experimentally investigated in terms of vapour-liquid equilibrium measurements [26] by using a VLE cell. Then, the obtained VLE data have been used for the thermodynamic assessment of the mixture and to achieve a reliable thermal efficiency of the power cycle in CSP application at 823 K turbine inlet temperature. Recently, given the outstanding thermal stability of perfluorocarbons, the CO_2 mixture with c-C_4F_8 have been investigated [27] as potential working fluid in transcritical power cycles in CSP plants with central receiver. However, in the latter reference, no experimental VLE data were available to optimise the thermodynamic model, so the uncertainty in the performance results is not negligible. Additionally, the absence of experimental data on the phase behaviour of the mixture prevents an accurate determination of the minimum cycle pressure, specifically the bubble pressure at the pump inlet's minimum cycle temperature. The presence of even a few VLE points in the mixture enables more precise studies to ascertain its potential in power cycles. This article is intended to present a newly developed apparatus for bubble point measurements, that allows the investigation of new potential CO_2 mixtures for thermodynamic cycles with the need for limited equipment compared to traditional VLE and PVT systems abovementioned.

The isochoric apparatus developed in the Fluid Test Laboratory of the University of Brescia [28], which is presented and validated in the following sections. The experimental setup is designed to obtain bubble points of mixtures from the divergence of isochoric behaviour of the mixture between the two-phase VLE region and the single-phase liquid region. The apparatus implemented in our laboratory employs a methodology (isochoric) already established in the literature; however, the proposed isochoric system provides the advantage of a simplified procedure and equipment, resulting in reduced cost.

Hall and Eubank [29] showcased the viability of the isochoric technique for acquiring VLE data of mixtures, employing a sophisticated experimental setup inspired by the Burnett method [30]. The Burnett method is characterised by a series of isothermal expansions performed on the fluid; this technique involves transferring the fluid from an initial volume to a pre-evacuated secondary volume, and pressure measurements are recorded after each expansion. To date, the Burnett method still ranks as one of the most precise techniques for determining PVT

behaviour. As stated by Hall and Eubank, "a rough PVT apparatus can reproduce conventional VLE data within the accuracy of the latter" [29], referring to a conventional VLE apparatus. Stouffer et al. [31] modified the apparatus described by Hall and Eubank including a small density reduction cell to expand the CO_2+hydrogen sulphide mixture from homogeneous liquid condition, and therefore investigating multiple isochores above the critical one. This modification, enabling the exploration of multiple isochores through expansion in the liquid phase, facilitated the acquisition of multiple bubble points for the mixture. Each isochore corresponds, in fact, to a unique bubble point of the mixture. Then, Zhou et al. [32] developed an automated isochoric apparatus for vapour-liquid equilibrium and density measurements of natural gas-like mixtures. The interesting apparatus is well described in his PhD dissertation [33], however only dew points were measured and, compared to our setup, the procedure required the externally preparation of the mixture to be charged in the cell at each investigated isochore. Also Velez et al. [34] adopted a constant-volume (isochoric) system to obtain phase transition points for methanol + vegetal oils, reacting systems, from the intersection of the isochoric lines. Recently, Goni et al. [35] adopted the isochoric methodology to measure bubble points of binary mixtures of ethane with heavy hydrocarbons (decane, undecane, dodecane and tridecane), proving good agreement between their data and previous isothermal VLE measurements in literature.

Compared to the abovementioned isochoric investigations, the VLE setup, presented in this work, is characterised by a simple design and a reduced number of components (sensors, valves, fittings), making it feasible for less-equipped laboratories, without compromising on flexibility to different binary mixtures and accuracy. Moreover, a straightforward procedure to fill the vessel and change the mixture density without compromising the composition is here discussed. The proposed methodology has been validated through the measurement of bubble points of well-known CO_2 binary mixtures with C_6F_6 and n-pentane, proving its consistency with previously published experimental VLE data. Afterwards the apparatus has been used to determine experimental bubble of the mixture CO_2+c-C_4F_8, never published before, at a composition relevant to transcritical power cycle considerations. Amongst the various perfluorocarbons investigated in the H2020 Scarabeus project, the CO_2+c-C_4F_8 mixture was recently examined by Morosini et al. [27] in a CSP plant with central receiver, operating at a turbine inlet temperature of 823 K. However, the referenced study lacked available VLE data, raising concerns about the optimisation of the thermodynamic model and the reliability of the design conditions and efficiency values. The thermodynamic model has been fine-tuned based on the obtained experimental data in this work, ensuring a robust evaluation of the power cycle and providing reliable design point for the component manufacturing.

2. Experimental investigation

In this section, the experimental setup will be presented, as well as the methodology adopted for the bubble point determination. The mixture preparation procedure will be discussed after a description of the apparatus, as the mixture is directly prepared within the system rather than in an external cylinder.

2.1. Chemicals

The chemical species that have been experimentally investigated are reported in Table 1, along with their commercial supplier and purity level. The chemicals have been used without further purification.

2.2. Experimental setup

The schematic of the apparatus in its main components is presented in Fig. 1. The core of the apparatus consists of a flanged cylinder made of stainless steel SS304, sealed with 8 bolts and an inert graphite gasket ("d" in Fig. 1). The cylinder has been designed for a maximum temperature of 503 K and a maximum pressure of 25 MPa. The lowest temperature that can be explored is 228 K, according to the refrigeration limits of the cryostat. The total internal volume, including tubing and other cavities, resulted to be 127.6 mL, evaluated by weighting the cell fully charged with distilled water compared to the empty vessel at vacuum conditions. Before each test, the system undergoes a leak testing with pure CO_2 at 4.5 MPa for a prolonged period of time (3 days).

Table 1
Investigated chemicals with information about suppliers and purity.

Component	CAS number	Supplier	Purity [% mol]	MW [g/mol]
CO_2	124-38-9	Sol [36]	99.99	44.01
C_6F_6	392-56-3	Alfa Aesar [37]	>99	186.06
C_5H_{12}	109-66-0	Sigma-Aldrich [38]	98	72.15
c-C_4F_8	115-25-3	Abcr GmbH [39]	99	200.03

The system is placed inside a thermostatic bath (Julabo FP40, represented by red dotted line in Fig. 1), to ensure a stable temperature control. The temperature of the bath is set by a PID controller and can be varied from 228 K to 423 K, with a resolution of 0.1 K.

A LabVIEW program is used for the acquisition and recording of temperature and pressure signals. The temperature is acquired with a 4-wires thermoresistance Pt100 with tolerance ±0.03 K at 273 K (class 1/10), while ±0.08 K at 373 K, which is inserted in the housing "b" in Fig. 1.

The pressure transducer is the model PA-33X manufactured by Keller, with digital interface RS485. The instrument has undergone dedicated calibration within the temperature range of 293–393 K (9 points) to ensure high accuracy across the entire temperature range of interest. An additional calibration was performed by an accredited calibration laboratory. The full scale (FS) of the pressure transmitter is 10 MPa (absolute). The total error band resulting from the calibration procedure ranges from -0.002 %FS (293 K) to 0.007 %FS (393 K).

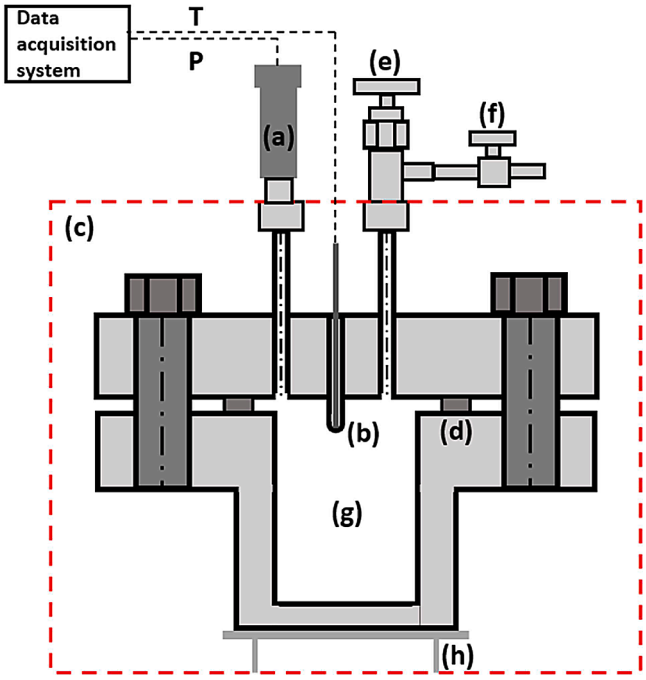

Fig. 1. Schematisation of the apparatus adopted for the bubble-points measurements: (a) pressure transducer; (b) thermoresistance well with temperature probe; (c) boundaries of thermal oil - thermostatic bath; (d) graphite gasket; (e) cell main valve; (f) charging/venting valve; (g) cell internal volume; (h) cylinder support.

Moreover, the pressure transmitter also measures the temperature behind its metallic separating diaphragm, with a resolution of ±2°K, but this information is recorded only to ensure that isothermal conditions are reached in all the vertical sections of the apparatus.

Isothermal conditions can be met in the cell thanks to the compact design considering that the internal volume ("g" in Fig. 1), thus the investigated the fluid is completely submerged into the thermostatic bath. A metallic support ("h" in Fig. 1) has been adopted to regulate the cylinder elevation with respect to thermal oil, in order to prevent the pressure transducer from wetting and the consequent overheating of the electrical components. Then, the top of the system is covered with rockwool to minimise the heat transfer with the environment.

2.3. Mixture preparation

Following the description of the experimental setup, it is here discussed how the mixture is directly prepared into the cell. Compared to many literature approaches [40], in this procedure there is no need for an external pressurised cylinder above the bubble pressure, at ambient temperature, to maintain the mixture in a homogeneous liquid phase while charging the cell. This approach avoids additional costs and the risk of the pressurizing gas (usually nitrogen) leaking through the piston into the mixture, usually determined by piston seal degradation over time.

The components of the mixture are charged into the cell according to their relative volatility. In case of CO_2 binary mixture with higher critical point dopant, the latter is charged first in the cell. Before the loading phase, air is evacuated from the system to around 100 Pa with a DamiCosmos vacuum pump, and the system is weighted with a Mettler-Toledo MS-TS Precision scalewhich has an accuracy of ±0.01 g. As the cell volume is quite big (approximately 127.6 mL), the typical amount of each component is in the order of tens of grams, then the uncertainty on the composition, given by the weighting, is negligible: the only contribution of composition uncertainty is given by the declared purity of the fluid samples from manufacturer (Table 1).

The desired mass of the first component is introduced into the system, and subsequently the vacuum pump is used for few seconds to remove the potential non-condensable gases dissolved in the fluid sample. The main valve ("e" in Fig. 1) is then closed and the confined fluid between valve "e" and "f" is entirely removed with the vacuum pump. The resulting mass of the competent is so determined weighting again the apparatus and deducting the tare measurement. The mass of each component charged into the system is specified in Appendix B.

Then, the CO_2 is charged from the bottle with a proper pressure reducer in order to charge the target mass of CO_2 at controlled temperature and pressure (then density). The piping that connects the CO_2 bottle and the cell is under vacuum conditions before charging, to avoid air intake in the cell. The weight of the system filled with the mixture is then measured again, and the resulting mixture composition is computed.

The charging procedure starts from the definition of the target composition to be investigated. At the same time, the mass of each component to be charged is constrained to achieve the target value of density in order to investigate an isochoric sufficiently higher than the critical density of the mixture.

2.4. Methodology description

After the charging procedure is completed, the mixture is in two-phase vapour-liquid equilibrium region, at density higher than the critical one. The physical principle that allows to determine the bubble points of the mixture with this apparatus is the relative change in compressibility between the liquid phase and the two-phase mixture, that in an isochoric system can be visualised as the slope of the pressure against the temperature (dP/dT). As can be seen for a generic binary mixture in the p-T plane in Fig. 2, the single-phase liquid mixture is less compressible than the two-phase mixture, leading to high pressure variation as consequence of a temperature variation. Accordingly, the bubble point (bubble pressure and temperature) can be determined by the intersection of the isochoric line both preceding and following the bubble temperature. The same methodology based on the interception between the lines that best fit the experimental points, in the VLE and liquid regions, is adopted also

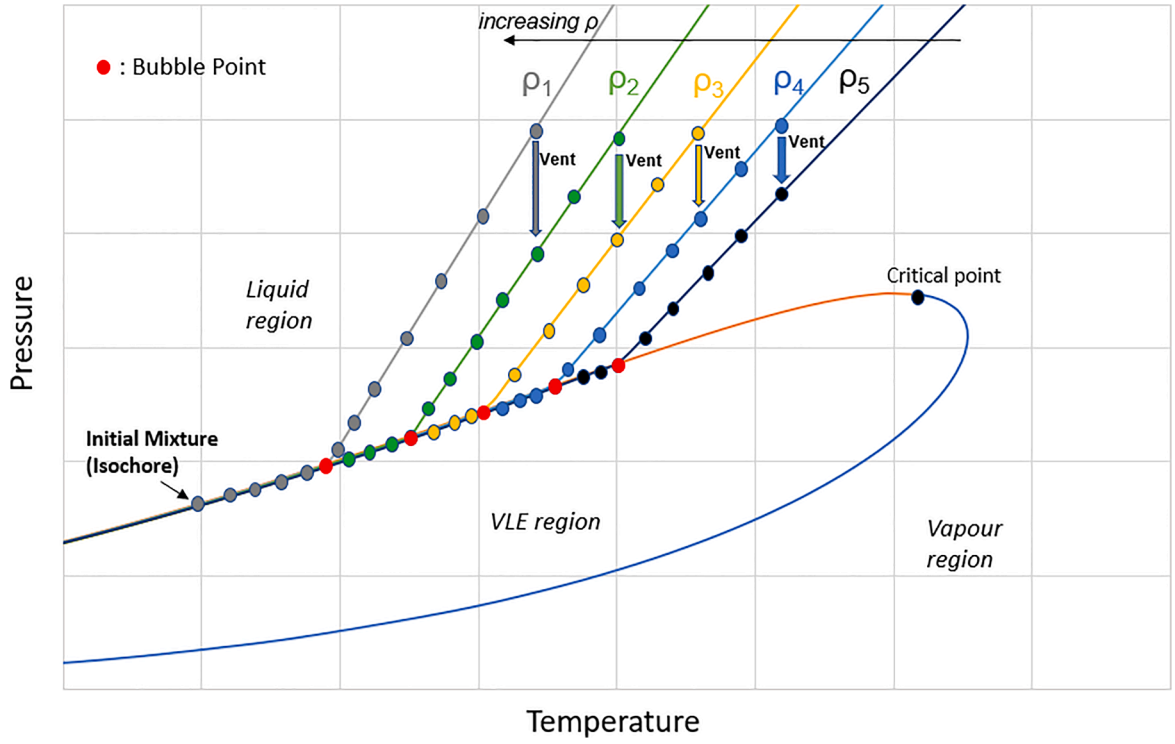

Fig. 2. Conceptual procedure for the bubble point identification of a mixture using an isochoric setup, with dots representing each experimental (P,T) measurement, different colours stand for different series (isochores) measured, and the simulated phase envelope and critical point; the bubble points (red dots) are identified from the drastic change in slope of the isochore between the VLE region and the single-phase liquid region.

in variable-volume PVT apparatus. In the latter case, compared to an isochoric apparatus, the bubble point is identified as interception point in the pressure-volume plane [40,41]. The same procedure could be used to measure the dew points of a mixture in case the mixture is charged in the cell at a density lower than the critical one.

For each isochore investigated, it is possible to obtain one single bubble point of the mixture charged in the cell. For this reason, as presented in Fig. 2, a venting of a small portion of the homogeneous liquid mixture is carried out in high-pressure conditions. By actuating the main valve ("e" in Fig. 2), the liquid mixture is introduced into the confined piping volume between valves "e" and "f", causing a minor pressure reduction. That volume is around 2 mL (1.5 % of the cell volume), then it causes a little pressure drop in the cell, which prevents the mixture from entering the VLE region and undergoing phase separation. Following this, valve "e" is closed, and the small portion of the mixture is evacuated under hood by opening valve "f." This procedure is reiterated until the desired temperature and pressure conditions are achieved for a new isochoric investigation, at a lower mixture density compared to the previous one. This simple technique allows to perform the same concept introduced by Stouffer et al. [31], with their density reduction cell in the modified Burnett apparatus, but in a much simpler manner. Moreover, by adopting this approach, there is no need for an external pressurised cylinder to charge the mixture in the cell at a different density.

Upon achieving equilibrium, the temperature and pressure measurements are typically recorded when the standard deviations for pressure and temperature are below 3 mbar and 0.001 K, respectively, for two minutes recording time.

After acquiring one measurement, the temperature is systematically incremented, and the system is allowed to reach a new equilibrium state (P,T) along the isochoric line.

It must be stressed out that, at high reduced densities ($\rho >> \rho_{cr}$), as evident in Fig. 2, each single experimental point (P,T) measured in the VLE region lies very close to the bubble line and could be considered as a qualitative bubble point of the mixture itself. Even if the difference between the experimental points in the VLE region and the bubble curve is within the experimental uncertainty, in this work only the bubble points obtained from the curves interception are proposed. The earlier assertion is emphasised to underscore that, regardless of the isochoric line's slope in the liquid region, the intersection point invariably aligns with the bubble line. This means that the rigorous mathematical uncertainty detailed in the Appendix A is misleading, as it fails to capture the physics elucidated in this work and the efficacy of the proposed method.

3. Experimental results, modelling, and discussion

The experimental campaign consists of the determination of the bubble points of three CO_2 based binary mixtures identifying the interception between the two-phase and the liquid region at different density and compositions. Two mixtures (CO_2+C_6F_6 and CO_2+C_5H_{12}), whose volumetric behaviour is well-known in literature, are selected to validate the proposed apparatus and procedure while VLE data on the blend CO_2+c-C_4F_8 are here presented for the first time. As already mentioned, the interest on this blend relies on its adoption as working fluid in closed power cycle for CSP or other applications.

The bubble points, measured with the procedure presented in the previous section, are reported in Appendix B, with the associated uncertainty computed as in Appendix A. The results are also presented in graphical form in the next sections.

The validation of the first two blends is performed indirectly comparing the experimental results with suitable thermodynamic model, fitted with previous literature measurements. This expedient Is necessary because the mixture compositions obtained by the loading procedure are close but different from the ones available in literature: it is so important to verify that the experimental results are aligned with the one used to characterise the mixture behaviour in literature.

The original PR EoS [42], as expressed in Eqs. (1)-(6), has been considered for the post-processing and comparison of the experimental data, given its simplicity and robustness.

$$P = \frac{RT}{v-b} - \frac{\alpha a}{v(v+b)+b(v-b)} \tag{1}$$

where the alpha function adopted is in its original form [42]:

$$\alpha = \left[1 + k\left(1 - \sqrt{T_r}\right)\right]^2 \tag{2}$$

$$k = 0.37464 + 1.54226\omega - 0.26992\omega^2 \tag{3}$$

$$a = 0.45724\frac{R^2 T_{cr}^2}{P_{cr}} \tag{4}$$

$$b = 0.0778\frac{RT_{cr}}{P_{cr}} \tag{5}$$

Van der Waals mixing rules are then adopted to describe the binary mixture as follows:

$$a_m = \sum_{i=1}^{n_c}\sum_{j=1}^{n_c} x_i x_j \sqrt{a_{ii}a_{jj}}\left(1 - k_{ij}\right) \tag{6}$$

$$b_m = \sum_{i=1}^{n_c} x_i b_i \tag{7}$$

where the binary interaction parameter k_{ij}=k_{ji} must be fitted on available vapour-liquid equilibrium data to improve the accuracy of the EoS in the mixture description.

The BIP regression is performed within the software ASPEN Properties v12 [16], using the maximum likelihood method as numerical optimisation method. The Britt–Luecke algorithm [43] with Deming initialisation method [44] was applied to regress the parameter. The Average Absolute Deviation percentage (AAD%) is selected as a metric to quantify the Equation of State (EoS) fitting capability for the experimental data. The AAD percentage is computed in this work as shown in Eq. (8), where P_{exp} is the measured value, P_{calc} is the value calculated by using the optimised EoS and N is the number of experimental data considered:

$$AAD_{Pbubble}[\%] = \frac{100}{N}\cdot\sum_{i=1}^{N}\left|\frac{P_{exp} - P_{calc}}{P_{exp}}\right| \tag{8}$$

The consistency of bubble points measured in this study is assessed by comparing the AAD percentage of a thermodynamic model tuned with literature data against the bubble points measured here. If the AAD of the model with our data is equal or lower than that with literature data, the bubble points obtained in this work are considered in good agreement with the literature.

The parameters of the chemical species studied in this work that are required by the PR EoS are reported in Table 2.

3.1. CO_2+C_6F_6 mixture

The CO_2+C_6F_6 mixture is one of the two reference mixture here selected for the methodology and procedure validation. According to a

Table 2
Parameters adopted by the EoS (default values in Aspen Properties [45]) and the BIPs of the mixtures.

Component	T_{cr} [K]	P_{cr} [MPa]	ω [-]	BIP CO_2 mixture
CO_2	304.21	7.383	0.224	–
C_6F_6	516.73	3.273	0.396	k_{ij} = 0.16297–0.0003951·T [K] [26]
C_5H_{12}	469.7	3.37	0.252	k_{ij} = 0.1222*
c-C_4F_8	388.37	2.778	0.356	See Section 3.3

* Default value in Aspen Plus database, aligned with [46].

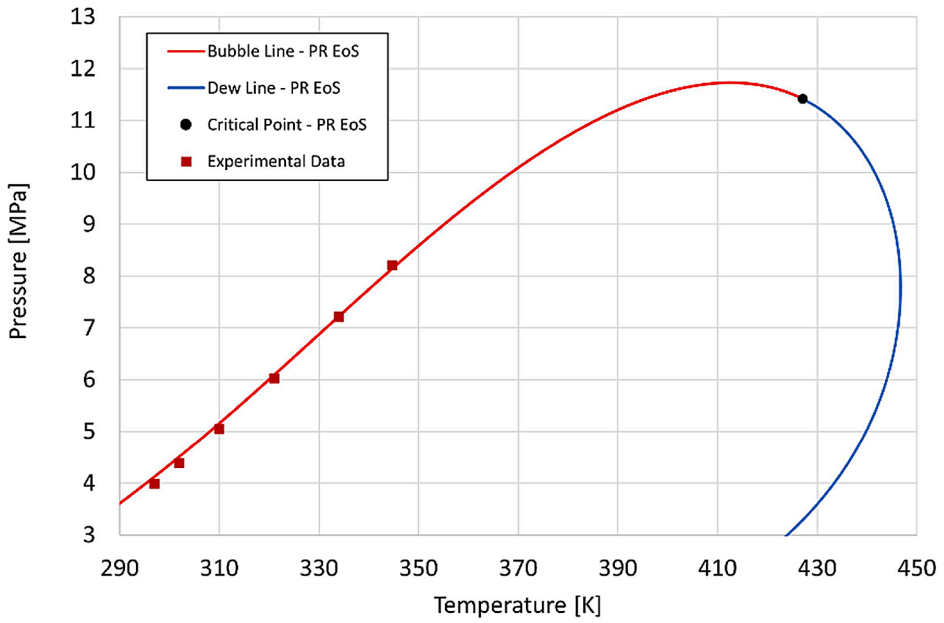

Fig. 3. Phase envelope (solid line) of the CO_2+C_6F_6 mixture (71.2 % molar CO_2) simulated with the PR EoS with k_{ij}, and the experimental data obtained in this work (red points).

previous experimental work of Di Marcoberardino et al. [26], the PR EoS is the EoS that guarantees the lowest average absolute deviation percentage (AAD = 2.6 %) when compared to experimental bubble pressures of the binary system CO_2+C_6F_6. The PR EoS as optimised in [26], with a temperature-dependent BIP equal to k_{ij} = 0.16297–0.0003951 T [K], has been considered to compare the data obtained in this work with the previous experimental data. The comparison is also available in graphical form in Fig. 3.

The mixture is loaded in the experimental apparatus at a 71.2 % CO_2 molar fraction. This composition aligns with the composition range of interest for the specific mixture in power cycle applications [26] and with available experimental data in the literature.

The experimental bubble points obtained in this work (red dots in Fig. 3), have an AAD% equal to 1.76 % compared with the PR EoS with k_{ij} as optimised in [26], which is lower than the AAD% reported by the model when compared to the experimental bubble points used in the fitting in the latter work (2.8 %), underscoring an agreement with the literature data.

3.2. CO_2+n-pentane mixture

The CO_2+n-pentane mixture has been investigated at two different molar compositions (data in Appendix B) with the aim to validate the procedure as well as to provide new experimental data. Specifically, we have focused on two compositions with molar fractions close to 50 %, where mixing effects are more pronounced: the resulting compositions, after the mixture preparation procedure and weighting, consist of a CO_2 fraction of 52.2 % and 62.3 %.

Besserer and Robinson [47] suggested that the earlier VLE data of Poettmann and Katz [48] regarding this binary mixture were inaccurate. They identified a significant discrepancy, exceeding 30 %, in the liquid phase compositions between their findings and those of Poettmann. Subsequently, Cheng et al. [46] conducted measurements on the CO_2+n-pentane binary system across a broader range of temperature and composition. Since their results were consistent with those of Besserer & Robinson, the data from Poettman and Katz have not been considered in this analysis.

For the CO_2+Pentane binary mixture, in Aspen Plus v12 environment, the BIP of the PR EoS is already available at the default value of k_{ij}=0.1222, which is a value considered also by Cheng et al. [46]. However, Cheng et al. [46] found out that no cubic EoS (Soave-Redlich-Kwong, Peng-Robinson, Kubic-Martin, and Adachi-Lu-Sugle) was able to correlate the data within the experimental error, even with the use of a BIP. An attempt to improve the capability of the EoS is performed here, regressing a temperature-dependent BIP on the experimental data of Cheng et al. [46], which resulted to be $k_{ij}(T)$ = 0.09396 + 0.00007878 T[K].

The predictive capability of the PR EoS for the VLE data measured by Cheng et al. [46] above 20 °C is illustrated by the average absolute percentage deviations shown in Fig. 4. It is worth noting that the data from Cheng et al. were selected as they constitute the largest dataset available for this mixture. In Fig. 4, also the deviations of the Kunz-Wagner EoS [49], as implemented in REFPROP v10 [50], are shown. A marginal improvement in the performance of the EoS is observed with the temperature-dependent BIP proposed here, resulting in an overall percentage AAD percentage of 1.9 %, compared to 2.3 % with the constant BIP. It's noteworthy that the AAD % reported by the REFPROP model is substantially higher at 4.3 %. Additionally, it's important to mention that several experimental points were excluded from the evaluation due to the REFPROP model's failure to converge under specific conditions. The model of REFPROP was applied by Ganesan and Eikevik [51] to analyse the performance of a cascaded high-temperature heat pump adopting CO_2+*n*-pentane mixture as working fluid in the topping cycle. However, the non-negligible error of the model implemented in REFPROP database at calculating the bubble pressure at elevated temperature suggests that it is not the best choice for the design of high-temperature heat pumps operating with CO_2+n-pentane binary mixture.

The AAD percentage of the PR EoS with temperature-dependent BIP against the bubble points measured in this work is equal to 2.9 %, which is aligned with the deviations of the thermodynamic model compared to literature data (see Fig. 4).

To enable a visual comparison, points were extrapolated from the obtained bubble lines in this study, aligning them with the same temperatures as other isothermal VLE datasets available in the literature. This comparison is shown in Fig. 5. The bubble points, extrapolated from the measured bubble, line are consistent with the data of Cheng et al. [46] and perfectly aligned with the data of Besserer & Robinson [47]. This provides further evidence of agreement between the data obtained in this study and the data reported in earlier literature works.

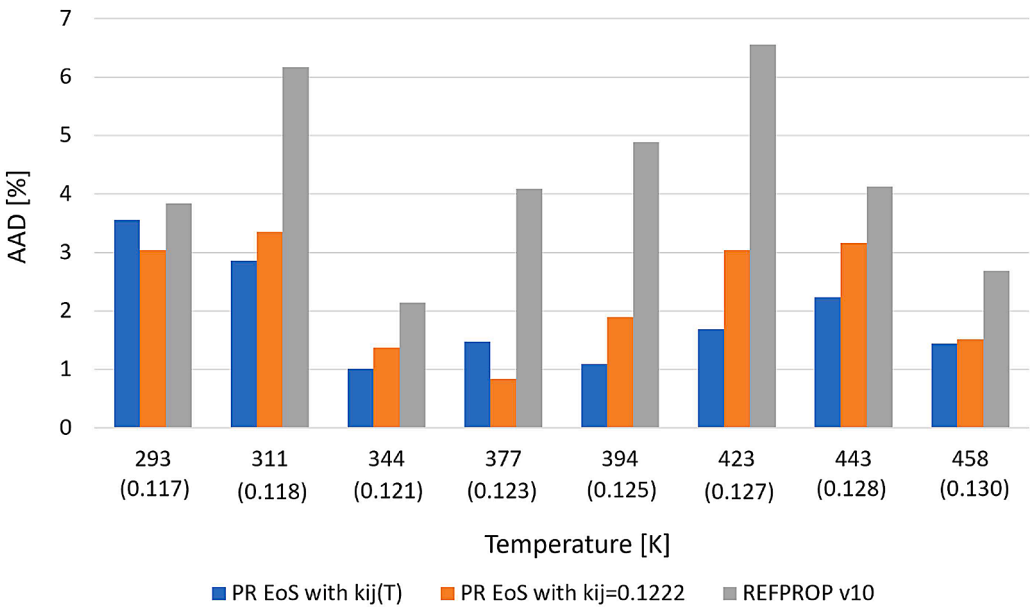

Fig. 4. Average absolute deviation of different EoS compared to the VLE data measured by a previous literature work (Cheng et al. [46]) above 293 K; on the temperature axis, the values of the $k_{ij}(T)$ are reported within brackets.

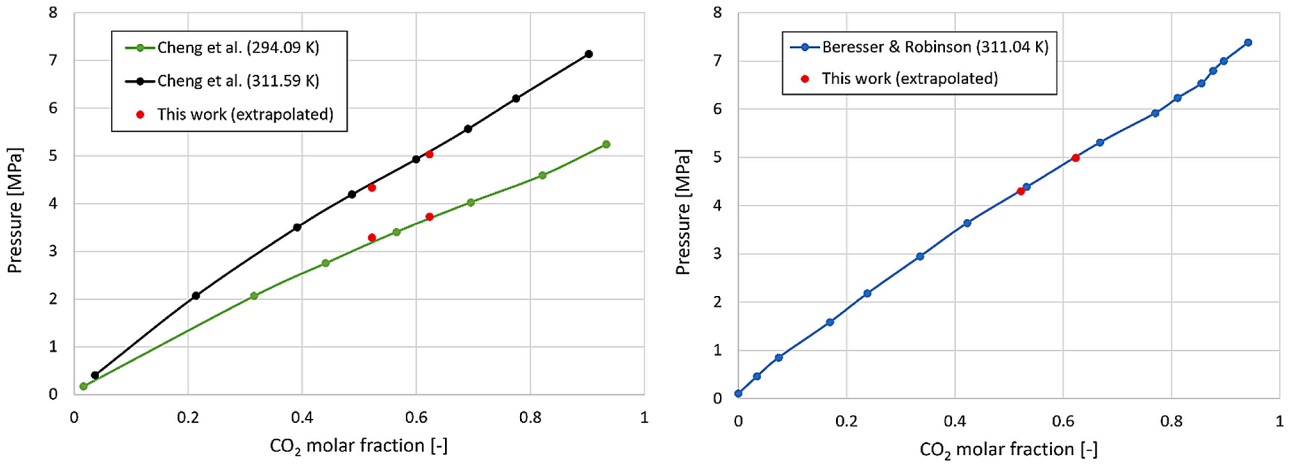

Fig. 5. Bubble points measured by other authors in the literature, and the bubble points extrapolated from the measurements of this work (red dots) at the same temperatures.

3.3. CO_2+c-C_4F_8 bubble points and EoS tuning

After validating the setup and procedure, bubble points of the CO_2 mixture with c-C_4F_8 have been measured at a composition of interest from the power cycle point of view [27], specifically at 77.25 % CO_2 molar fraction. The bubble points, along with their uncertainty, are reported in Appendix B. In this case, the experimental measurements are required to calibrate, for the first time, the BIP of a suitable EoS.

Table 3 presents the BIP (k_{ij}) acquired through data regression in Aspen Plus v12, along with the AAD percentage computed on the bubble pressure for each temperature. The table also includes an overall average AAD %, which results to be 0.31 % for PR EoS with van der Waals mixing rules. For comparison purposes, the same procedure for the BIP regression is carried out for PR EoS with Boston Mathias (PR-BM) alpha function [52], PR EoS with Wong Sandler (PR-WS) mixing rules [53], and Soave-Redlich-Kwong EoS [54]. The deviations compared to experimental data are reported in Table 3.

In Fig. 6 all the measurements (both in VLE and liquid regions) used to obtain the bubble points are reported. The phase envelope, in Fig. 6, calculated with the PR EoS as optimised in this section on the experimental bubble points (k_{ij} = 0.0407) shows the good agreement with the experimental data. It can be noted, instead, that the phase envelope calculated without EoS optimisation (k_{ij} = 0) leads to errors in calculating the bubble line, as well as in the estimation of the critical point of the mixture. The lowest isochore investigated in Fig. 6 is too close to the critical point to determine with good accuracy the bubble point: the density of the vapour and liquid phase are similar approaching the critical point. For this reason, this bubble point is not considered nor reported in Appendix B.

As mentioned in the methodology section, the distance of each experimental point in the VLE region (blue dots in Fig. 6) to the bubble line is within the instrumental uncertainty, for the isochores at low reduced temperature. For this reason, each individual point effectively could be considered as a standalone bubble point. However, this perspective is not explored in this study, and the bubble point is reported only as intersection between the VLE and liquid isochoric lines.

Table 3
BIP regressed and AAD% of different EoS vs experimental bubble points of CO_2+c-C_4F_8 mixture.

EoS	k_{ij}	AAD percentage				
		282.95 K	295.25 K	309.75 K	317.05 K	Average
PR-vdW	0.04070 ± 0.00398	0.3 %	0.28 %	0.62 %	0.06 %	0.31 %
PR-BM	0.03946 ± 0.00252	0.33 %	0.21 %	0.76 %	0.56 %	0.34 %
PR-WS	0.42052 ± 0.018511	3.09 %	1.53 %	0.68 %	3.79 %	2.27 %
SRK	0.04442 ± 0.00389	4.34 %	4.44 %	4.91 %	3.75 %	4.33 %

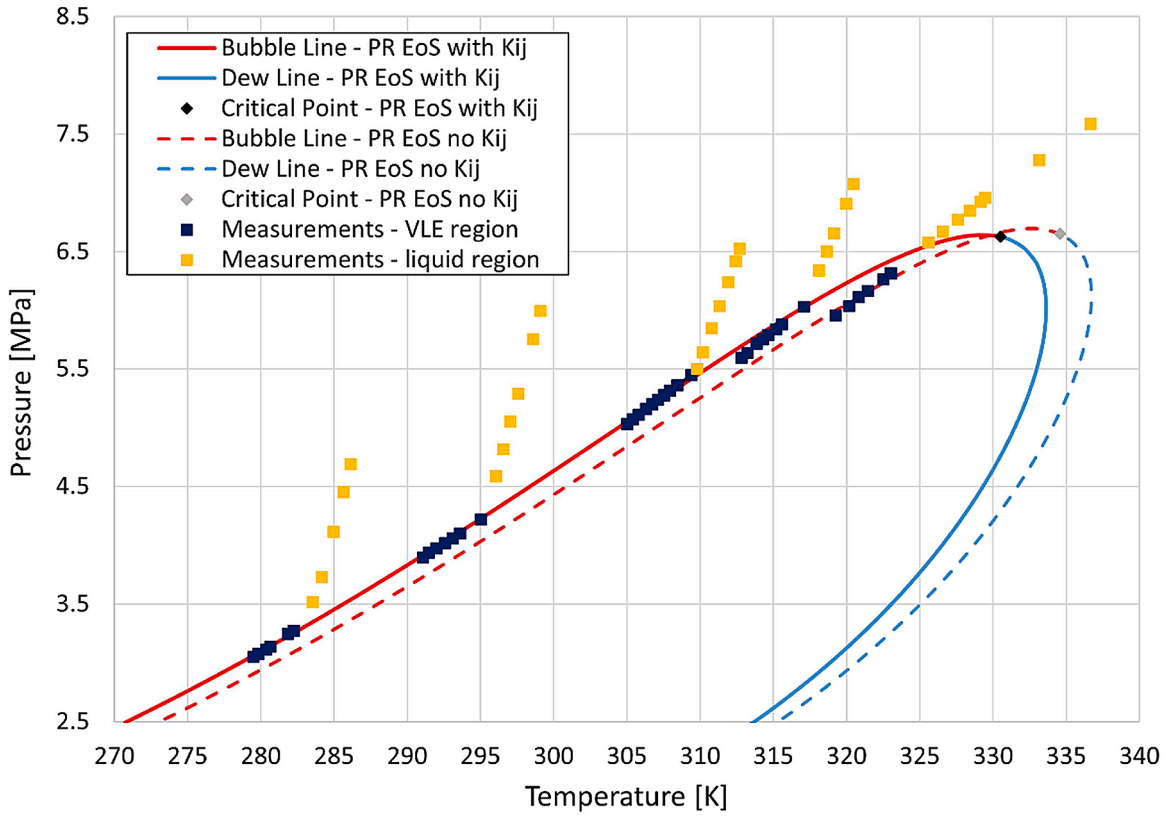

Fig. 6. Experimental measurements of CO_2+c-C_4F_8 mixture (77.25 % molar CO_2), and the phase envelope calculated both with the PR EoS optimised on the bubble points (k_{ij} = 0.0407) and without BIP (k_{ij} = 0).

4. Application of the mixture CO_2+c-C_4F_8: power cycle modelling

In this section, the PR EoS, optimised on the bubble points obtained in this work, will be used to evaluate the performance of the CO_2+c-C_4F_8 mixture in a CSP tower plant.

Over the last years, perfluorocarbons have been proposed as suitable dopant for blending CO_2 as working fluid for CSP tower power block because of the potential high thermal stability related to the C-F bond energy. The mixture CO_2+c-C_4F_8 was already presented in a previous work [27] showing interesting power cycle efficiency values although it wasn't possible to optimise the property model due to the lack of information in literature about the phase behaviour (i.e. the molecules interaction). The experimental campaign carried out on this mixture aimed at covering this gag: the PR EoS with vdW mixing rules, as optimised in the previous section (k_{ij} = 0.0407) on the experimental bubble points, is used here for the calculation of the thermodynamic properties of the mixture. The analysis presented here is therefore useful to validate the promising results of the mixture in CSP application.

The CO_2+c-C_4F_8 mixture operates in a transcritical power cycle in simple-recuperated (SR) and recompression (RC) layouts. The cycle is simulated in Aspen Plus V12 [45] with the assumptions reported in Table 4, which are in agreement with the previous study about this mixture [27]. The turbine inlet temperature (TIT) is equal to 823.15 K, coherently with a state-of-the-art CSP tower plant adopting molten salts as heat transfer and storage fluid.

The maximum cycle pressure at the pump outlet is dictated by the assumed turbine inlet pressure and the pressure drops across the heat exchangers on the high-pressure side. At fixed maximum pressure (mostly determined by material integrity at the maximum cycle temperature), the turbine pressure ratio and enthalpy drop at design conditions is determined by the bubble pressure and the design pressure

Table 4
Power cycles assumptions for CO_2+c-C_4F_8 mixture cycle.

Power cycle parameter	Value
Turbine inlet temperature [K]	823.15
Turbine Inlet pressure [MPa]	25.3
Cycle minimum temperature [K]	324.15
Turbine / pump isentropic efficiency [%]	92 / 88
PCHE minimum internal temperature difference [K]	5
Condenser pressure drop [MPa]	0.2
PHE pressure drop [MPa]	0.4
Recuperator pressure drop HP / LP [MPa]	0.05 / 0.1

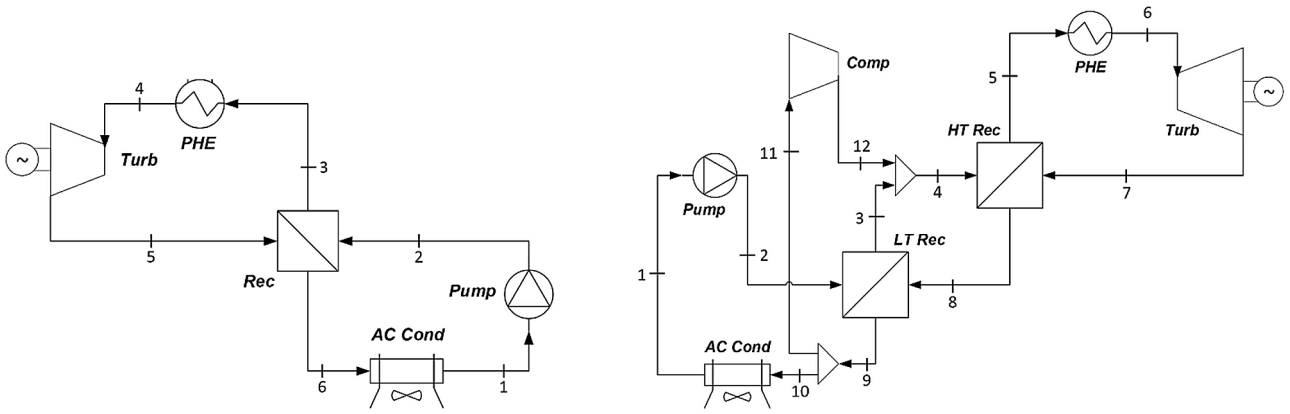

Fig. 7. Simple-recuperated (SR) on the left, and recompression (RC) layout on the right.

drops in the recuperator (or recuperators) and condenser. In this scenario, the accurate knowledge of the bubble pressure at fixed pump inlet is very relevant for the correct evaluation of the pressure ratio across the turbomachines.

The SR and RC cycle architectures are represented in Fig. 7, and the corresponding T-s diagram in Fig. 8. The mixture is pumped from the bubble point conditions up to the cycle maximum pressure, then it enters the recuperator to recover the thermal power available from the turbine outlet. After the internal heat recovery process, the mixture enters the primary heat exchanger (PHE) where it is heated up to 823.15 K by the molten salts. Then, the mixture is expanded in the turbine and cooled in the recuperator. In the end, the mixture enters the air-cooled condenser to condensate.

In comparison to the SR architecture, the RC configuration divides the internal heat recovery process into two heat exchangers handling different mass flow rates on the high-pressure side (cold side). Specifically, the turbine outlet stream sequentially passes through the High-Temperature (HT) Recuperator and Low-Temperature (LT) Recuperator before undergoing a separation: a portion enters the compressor, mixing with high-pressure steam at the LT Recuperator outlet, while the rest proceeds for complete condensation, undergoes pumping, and re-enters the LT Recuperator. The recompression layout is adopted to balance the heat capacities, then to reduce the irreversibility in the internal heat recovery process.

A sensitivity analysis is performed to assess the thermodynamic cycle efficiency at varying CO_2 molar content. The thermal efficiency of the simple recuperated (SR) and recompression (RC) cycles are defined according to Eqs. (9) and 10, respectively.

$$\eta_{th,SR} = \frac{W_{Turbine} - W_{Pump}}{Q_{in}} \tag{9}$$

$$\eta_{th,\ RC} = \frac{W_{Turbine} - W_{Pump} - W_{compressor}}{Q_{in}} \tag{10}$$

Results are reported in Fig. 9 according to the optimised thermodynamic model (PR EoS with k_{ij}) and the non-optimised model (PR EoS with null k_{ij}). The optimisation of the thermodynamic model confirms the good efficiency of the mixture under reliable design conditions, outperforming pure sCO_2 under the same assumptions and power block [27]. A maximum value of 43 % efficiency is reached when approaching the 50 % dopant molar content, in a simple recuperated architecture. Instead, the composition that optimise the RC cycle efficiency is around 27 % c-C_4F_8 molar content, surpassing the 44 % thermal efficiency. The thermodynamic model optimisation confirms, then, the good efficiency achieved with the adoption of this mixture.

Although the gap between the calculated design efficiency using an optimised and non-optimised thermodynamic model is low (less than 0.2 percentage points), as evidenced in Fig. 9, the difference on the prediction of the mixture density and enthalpy at different operating conditions may lead to notable inconsistencies in the design of each cycle components. Assuming a power block with a target mechanical output of 100 MW, Table 5 shows the impact of the BIP on the different

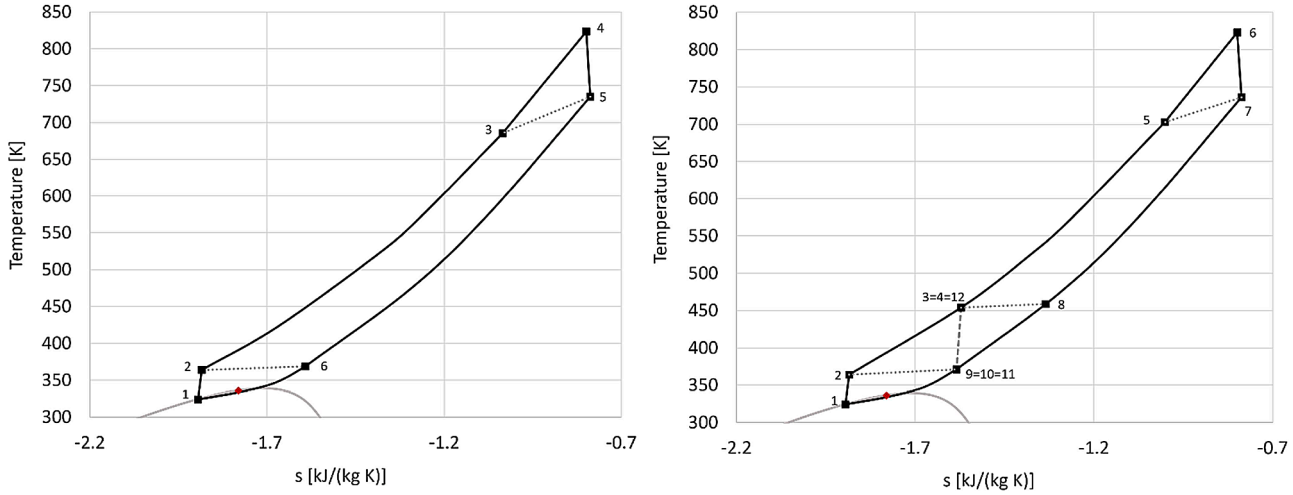

Fig. 8. T-s diagram of the transcritical cycle adopting CO_2+c-C_4F_8 mixture (27 % c-C_4F_8 molar fraction) in SR layout (left) and RC layout (right). The critical point of the mixture is represented as a red diamond in the T-s diagram. The internal heat recovery processes (LT and HT Rec) is represented through dotted lines, while the re-compression as dashed line.

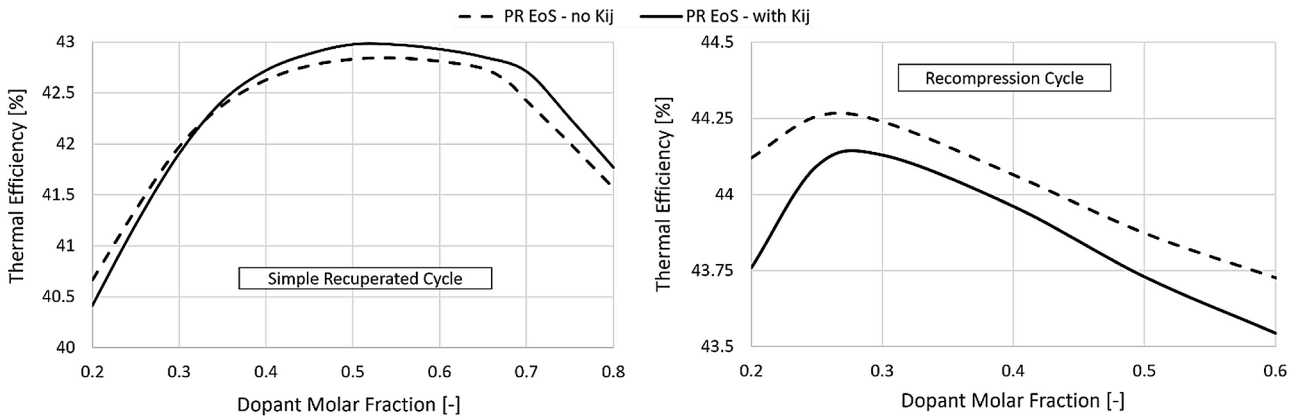

Fig. 9. Thermal efficiency of the CO_2+c-C_4F_8 cycle calculated both with the PR EoS optimised (k_{ij} = 0.0407) and without optimisation (k_{ij} = 0), in simple recuperated layout (left side) and recompression layout (right side).

Table 5
Percentage deviations on component design when performed with non-optimised PR EoS (k_{ij} = 0) compared to the optimised EoS (k_{ij} = 0.0407)), with 27 % dopant molar content and targeting the same mechanical output (100 MW).

Parameter	Percentage deviation (RC cycle) [%]	Percentage deviation (SR cycle) [%]
$P_{min,cycle}$	-3.25	-3.25
PHE thermal power	-0.3	-0.28
Mass flow rate	-3.27	-3.51
Turbine power	-1.4	-1.62
Pump power	-7.23	-6.37
Compressor power	-1.49	–
LT recuperator Th. power	-0.68	-3.08
HT recuperator Th. power	-3.85	–
UA LT recuperator	-2.8	-2.67
UA HT recuperator	-6.68	–
Condenser thermal power	-0.53	-0.49

components design with respect to a null kij for the two investigated layouts. The discrepancies highlight the errors that stem from designing components based on a non-optimised thermodynamic model.

Under similar thermal power exchanged in the primary heat exchanger (-0.3 %), the inconsistencies on components design are highlighted. Firstly, the minimum cycle pressure is underestimated by 3.25 % compared to the actual value required for the complete condensation of the mixture at 324.15 K (minimum cycle temperature). This implies that, in operation, the turbine (and then the other components) must operate under off-design conditions, expanding at a higher pressure to ensure full condensation of the mixture. This has an impact on the turbomachines and cycle efficiency, which can only be assessed through a proper off-design analysis, beyond the scope of this study. The heat exchangers appear as underestimated too: the UA product (representative of the size) of the recuperator, in particular, is noticeably lower (up to 6.7 %) than the actual value that guarantee the declared effectiveness, i.e. the 5 K as minimum pinch temperature. As a result, the heat transfer area obtained with incorrect design conditions would be underestimated, which penalises the effectiveness of the heat exchangers.

Also, the pump power results to be underestimated by 3.25 % when the power cycle is designed with null k_{ij} value, which mostly reflects the error in the determination of the correct mass flow rate of the mixture (3.27 %).

5. Conclusions

A novel isochoric apparatus is presented for the measurement of vapour-liquid equilibrium phase boundaries of mixtures. The experimental setup and procedure have been validated by measuring bubble points of CO_2 binary mixtures with hexafluorobenzene and n-pentane, characterised in previous literature works. Specifically, the absolute deviation of the PR equation of state, in comparison to the measured bubble points, was similar or even lower than the corresponding deviation observed when using the same thermodynamic model tuned on previous literature data.

Bubble points of the CO_2+c-C_4F_8 mixture, which have not been experimentally investigated in the literature, have been measured at a composition of interest from a transcritical power cycle perspective. These bubble points were utilised for the refinement of the PR EoS. As a result, the average absolute deviation of the fitted EoS against experimental bubble points resulted to be 0.31 %. The calibrated thermodynamic model has been used then to evaluate the transcritical power cycle operating with the mixture as a working fluid in CSP application considering 823.15 K as maximum cycle temperature.

As a matter of facts, the utilisation of the EoS without fine-tuning (null binary interaction parameter) tends to overestimate the pressure ratio across turbomachines by 3.25 %. Furthermore, in the non-optimised scenario, the design pump power and the UA product of the recuperator are underestimated by more than 6 %, thereby impacting the cycle efficiency under actual operating conditions. The thermal efficiency of the mixture overcomes the 44 % value in a recompressed architecture, making it a promising candidate for future research.

The experimental isochoric setup introduced in this work will be employed in future studies to measure VLE data of CO_2 mixtures for closed power cycles, heat pumps and refrigeration systems.

CRediT authorship contribution statement

M. Doninelli: Writing – original draft, Visualization, Validation, Software, Resources, Methodology, Investigation, Formal analysis, Data curation, Conceptualization. **G. Di Marcoberardino:** Writing – review & editing, Visualization, Project administration, Investigation, Data curation. **C. M. Invernizzi:** Writing – review & editing, Supervision, Investigation. **P. Iora:** Writing – review & editing, Supervision, Project administration, Funding acquisition.

Declaration of competing interest

The authors declare that they have no known competing financial interests or personal relationships that could have appeared to influence the work reported in this paper.

Data availability

Data will be made available on request.

Acknowledgements

This paper is part of the project HICLOPS "High-medium temperature closed power cycles for waste heat recovery and renewable sources" that has received funding from the MUR Progetti di Rilevante Interesse Nazionale (PRIN) Bando 2022 under grant No 2022HMZ39A. The authors thank Lorenzo Ghidini for his assistance in the LabVIEW modelling.

Appendix A. Uncertainty calculation

A rigorous procedure is adopted to determine the uncertainty of each bubble point computed from the inserseption of the isochoric line in the two-phase and liquid-phase regions.

The uncertainty on the bubble temperature and pressure is computed as in Equations E1–4, multiplied with a coverage factor of $k = 2$ in order to extend it to a confidence interval of 95 %:

$$u_{Expanded}(\pi_{bub}) = k \cdot \sqrt{(u_{Calibration}(\pi))^2 + (u_{Acquisition}(\pi))^2 + (u_{Repetition}(\pi))^2 + (u_{Fitting}(\pi))^2} \quad \text{(E1)}$$

where the generic π_{bub} stands for the bubble pressure (P_{bub}) and bubble temperature (T_{bub}).

The contributions of the uncertainty are calculated as follows:

$$u_{Calibration}(\pi) = \max(Measured\ (\pi) - Reference\ (\pi)) \quad \text{(E2)}$$

$$u_{Acquisition}(\pi) = \sigma(\pi_{acquisited}) \ (\quad \text{(E3)}$$

$$u_{Repetition}(\pi) = \frac{\sigma(\pi_{measured})}{\sqrt{n}} \quad \text{(E4)}$$

The contribution of the calibration in the uncertainty calculations is evaluated accounting for the calibration curve of the instrument compared with a reference value. The pressure transducer has undergone dedicated calibration within the temperature range of 293–393 K, utilizing 9 calibration points. This calibration process ensures the attainment of high accuracy throughout the entire temperature range of interest. The pressure transmitter operates with a full scale (FS) of 100 bar (absolute). The total error band, derived from the calibration procedure, spans from -0.002 %FS at 293 K to 0.007 %FS at 393 K. The contribution of calibration is then considered to vary linearly from with the temperature as represented in Fig. A.1.

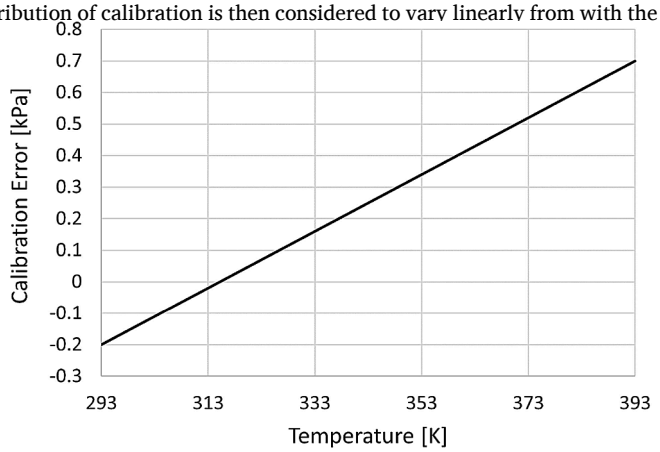

Fig. A. 1. Uncertainty contribution of the bubble pressure due to calibration procedure as function of temperature.

The contribution of the acquisitions to the uncertainties is accounted according to the standard deviation of the variable, $\sigma(\pi_{acquisited})$, directly computed with the data acquisition unit, in a wide range of at least 120 acquisitions with a frequency of one acquisition per second (2 min). Considering that the standard deviation of the single point acquired (over 2 min acquisition) is usually lower than 100 Pa and 0.0003 K, this uncertainty contribution is almost negligible. This is the result of the carefulness exercised in capturing each individual data point, allowing for the mixture to stabilise at the required temperature and pressure for the necessary duration.

The contribution of the repetition of each measurement to the final value reported (as an average) is accounted for the standard deviation of all the measured data $\sigma(\pi_{measured})$ divided by the square root of the number of data recorder at the same conditions (T,P,x).

Finally, it is introduced the fitting contribution ($u_{fitting}(\pi)$) related to the methodology used to obtain the bubble point (T_{bubble},P_{bubble}) from the inserseption of the isochoric lines fitting the measurements in the VLE and liquid regions. This contribution is calculated with the same rigorous mathematical procedure presented by Goni et al. [35] (in Appendix).

Appendix B. Experimental data

The bubble point data for the CO_2 mixtures, obtained through measurements using the isochoric apparatus in this study, are detailed in Tables T1–T3. These tables include information on the liquid molar fraction of CO_2, alongside the corresponding bubble temperatures and pressures, along with their expanded uncertainties. In Table T4 are reported the masses of each component charged into the cell along with its temperature during the CO_2 charging. The pressure at which the CO_2 is throttled during the transfer from its main bottle is also reported in Table T4. After charging, homogenisation of the mixture is ensured by waiting for at least 34 h. Then, the temperature is increased and venting in homogeneous liquid conditions is carried out up to the temperatures of interest in this work (above 280 K).

Table T1
Experimental bubble points for $xCO_2+(1-x)C_6F_6$ mixture.

CO_2 molar fraction [%]	T [K]	U(T) [K]	P [MPa]	U(P) [MPa]
71.2 %	297	0.08	3.987	0.015
	301.97	0.11	4.388	0.019
	310.04	0.08	5.049	0.011
	321.01	0.15	6.028	0.028
	334.01	0.15	7.211	0.034
	344.65	0.19	8.204	0.037

Table T2
Experimental bubble points for $xCO_2+(1-x)C_5H_{10}$ mixture.

CO_2 molar fraction [%]	T [K]	U(T) [K]	P [MPa]	U(P) [MPa]
	298.85	0.17	4.098	0.041
62.3 %	312	0.21	5.028	0.036
	327.47	0.62	6.225	0.096
	299.19	0.20	3.601	0.049
52.2 %	312.68	0.19	4.389	0.031
	329.5	0.28	5.478	0.054

Table T3
Experimental bubble points for $xCO_2+(1-x)c\text{-}C_4F_8$ mixture.

CO_2 molar fraction [%]	T [K]	U(T) [K]	P [MPa]	U(P) [MPa]
77.25 %	282.97	0.07	32.96	0.033
	295.3	0.05	42.38	0.011
	309.73	0.07	54.77	0.005
	317.09	0.17	60.25	0.27

Table T4
Masses of components charged for the preparation of the mixtures investigated.

Mix	x [molar%]	Mass CO_2 [g]	Mass [g]	Cell temperautre while charging CO_2 [K]	Pressure of CO_2 while charging [MPa]
$xCO_2+(1-x)C_6F_6$	71.2	56.05	95.83	258	2.5
$xCO_2+(1-x)C_5F_{12}$	62.3	48.350	47.960	263	2.85
$xCO_2+(1-x)C_5F_{12}$	52.2	37.34	56.02	263	2.85
$xCO_2+(1-x)c\text{-}C_4F_8$	77.25	59.74	79.98	283	5.0

References

[1] G. Angelino, Carbon dioxide condensation cycles for power production, J. Eng. Power. 90 (1968) 287–295, https://doi.org/10.1115/1.3609190.

[2] E.G. Feher, The supercritical thermodynamic power cycle, Energy Convers. 8.2 (1968) 85–90.

[3] V. Dostal, P. Hejzlar, M.J. Driscoll, High-performance supercritical carbon dioxide cycle for next-generation nuclear reactors, Nucl. Technol. 154 (2006) 265–282, https://doi.org/10.13182/NT154-265.

[4] M. Binotti, M. Astolfi, S. Campanari, G. Manzolini, P. Silva, Preliminary assessment of sCO2 cycles for power generation in CSP solar tower plants, Appl. Energy. 204 (2017) 1007–1017, https://doi.org/10.1016/j.apenergy.2017.05.121.

[5] D. Alfani, M. Binotti, E. Macchi, P. Silva, M. Astolfi, sCO2 power plants for waste heat recovery: design optimization and part-load operation strategies, Appl. Therm. Eng. 195 (2021) 117013, https://doi.org/10.1016/j.applthermaleng.2021.117013.

[6] M. Binotti, G. Di Marcoberardino, P. Iora, C. Invernizzi, G. Manzolini, Scarabeus: supercritical carbon dioxide/alternative fluid blends for efficiency upgrade of solar power plants, AIP Conf. Proc. (2020) 2303, https://doi.org/10.1063/5.0028799.

[7] DESOLINATION. Sustainable desalination from Concentrated Solar Power, 2021. https://desolination.eu/.

[8] G. Di Marcoberardino, C.M. Invernizzi, P. Iora, A. Ayub, D. Di Bona, P. Chiesa, M. Binotti, G. Manzolini, Experimental and analytical procedure for the characterization of innovative working fluids for power plants applications, Appl.

Therm. Eng. 178 (2020) 115513, https://doi.org/10.1016/j.applthermaleng.2020.115513.
[9] A.R. Imre, A.M. Ahmed, Effect of the working fluids critical temperature on thermal performance for trilateral flash cycle and organic Rankine cycle, Int. J. Thermofluids. 20 (2023) 100417, https://doi.org/10.1016/j.ijft.2023.100417.
[10] O.A. Terracciano, F. De Francesco, R. Brizzi, F. Annese, M. Doninelli, L. Putelli, M. Gelfi, An advanced desalination system with an innovative CO2 power cycle integrated with renewable energy sources, in: 2023: p. D011S017R002. https://doi.org/10.2118/215993-MS.
[11] A.S. Chowdhury, M.M. Ehsan, A critical overview of working fluids in organic rankine, supercritical rankine, and supercritical brayton cycles under various heat grade sources, Int. J. Thermofluids. 20 (2023) 100426, https://doi.org/10.1016/j.ijft.2023.100426.
[12] A.I. Turja, K.N. Sadat, M.M. Hasan, Y. Khan, M.M. Ehsan, Waste heat recuperation in advanced supercritical CO2 power cycles with organic rankine cycle integration & optimization using machine learning methods, Int. J. Thermofluids. 22 (2024) 100612, https://doi.org/10.1016/j.ijft.2024.100612.
[13] F. Crespi, G.S. Martínez, P.R. De Arriba, D. Sánchez, F. Jiménez-Espadafor, Influence of working fluid composition on the optimum characteristics of blended supercritical carbon dioxide cycles, Proc. ASME Turbo Expo. 10 (2021) 1–11, https://doi.org/10.1115/GT2021-60293.
[14] B. Dai, C. Dang, M. Li, H. Tian, Y. Ma, Thermodynamic performance assessment of carbon dioxide blends with low-global warming potential (GWP) working fluids for a heat pump water heater, Int. J. Refrig. 56 (2015) 1–14, https://doi.org/10.1016/j.ijrefrig.2014.11.009.
[15] J. Gómez-Hernández, R. Grimes, J.V. Briongos, C. Marugán-Cruz, D. Santana, Carbon dioxide and acetone mixtures as refrigerants for industry heat pumps to supply temperature in the range 150–220°C, Energy (2023) 269, https://doi.org/10.1016/j.energy.2023.126821.
[16] M. Doninelli, E. Morosini, G. Gentile, L. Putelli, G. Di Marcoberardino, M. Binotti, G. Manzolini, Thermal desalination from rejected heat of power cycles working with CO2-based working fluids in CSP application: a focus on the MED technology, Sustain. Energy Technol. Assessments. 60 (2023) 103481, https://doi.org/10.1016/j.seta.2023.103481.
[17] C. Chen, W. Su, L. Xing, X. Lin, D. Ji, N. Zhou, A prediction model for the binary interaction parameter of PR-VDW to predict thermo-physical properties of CO2 mixtures, Fluid Phase Equilib 565 (2023) 113634, https://doi.org/10.1016/j.fluid.2022.113634.
[18] R. Abdel-Azim, Estimation of bubble point pressure and solution gas oil ratio using artificial neural network, Int. J. Thermofluids. 14 (2022) 100159, https://doi.org/10.1016/j.ijft.2022.100159.
[19] M. Doninelli, E. Morosini, G. Di Marcoberardino, C.M. Invernizzi, P. Iora, M. Riva, P. Stringari, G. Manzolini, Experimental investigation of the CO2+SiCl4 mixture as innovative working fluid for power cycles: bubble points and liquid density measurements, Energy 299 (2024) 131197, https://doi.org/10.1016/j.energy.2024.131197.
[20] P. Guilbot, A. Valtz, H. Legendre, D. Richon, Rapid on-line sampler-injector: a reliable tool for HT-HP sampling and on-line GC analysis, Analusis 28 (2000) 426–431, https://doi.org/10.1051/analusis:2000128.
[21] K. Djebaili, E. El Ahmar, A. Valtz, A.H. Meniai, C. Coquelet, Vapor-liquid equilibrium data for the carbon dioxide (CO2) + 1,1,1,3,3-pentafluorobutane (R365mfc) system at temperatures from 283.15 to 337.15 K, J. Chem. Eng. Data. 63 (2018) 4626–4631, https://doi.org/10.1021/acs.jced.8b00683.
[22] H. Madani, A. Valtz, C. Coquelet, A.H. Meniai, D. Richon, Vapor + liquid) equilibrium data for (carbon dioxide + 1,1-difluoroethane) system at temperatures from (258 to 343) K and pressures up to about 8 MPa, J. Chem. Thermodyn. 40 (2008) 1490–1494, https://doi.org/10.1016/j.jct.2008.06.002.
[23] N. Juntarachat, A. Valtz, C. Coquelet, R. Privat, J.N. Jaubert, Experimental measurements and correlation of vapor-liquid equilibrium and critical data for the CO2 + R1234yf and CO2 + R1234ze(E) binary mixtures, Int. J. Refrig. 47 (2014) 141–152, https://doi.org/10.1016/j.ijrefrig.2014.09.001.
[24] Z. Wu, R. Sun, L. Shi, P. Hu, H. Tian, X. Wang, G. Shu, Vapor-liquid equilibrium measurement and critical line prediction for carbon dioxide (CO2) + fluoroethane (R161) binary mixtures, J. Supercrit. Fluids. 207 (2024) 106205, https://doi.org/10.1016/j.supflu.2024.106205.
[25] M.S. Sadaghiani, A. Arami-Niya, B. Marsh, S.Z.S. Al Ghafri, E.F. May, Vapor-liquid equilibria for carbon dioxide + 3,3,3-trifluoropropene binary mixtures at temperatures between (288 and 348) K, J. Chem. Eng. Data. 66 (2021) 4044–4055, https://doi.org/10.1021/acs.jced.1c00297.
[26] G. Di Marcoberardino, E. Morosini, D. Di Bona, P. Chiesa, C. Invernizzi, P. Iora, G. Manzolini, Experimental characterisation of CO2 + C6F6 mixture: thermal stability and vapour liquid equilibrium test for its application in transcritical power cycle, Appl. Therm. Eng. 212 (2022) 118520, https://doi.org/10.1016/j.applthermaleng.2022.118520.
[27] E. Morosini, E. Villa, G. Quadrio, M. Binotti, G. Manzolini, Solar tower CSP plants with transcritical cycles based on CO2 mixtures: a sensitivity on storage and power block layouts, Sol. Energy. 262 (2023) 111777, https://doi.org/10.1016/j.solener.2023.05.054.
[28] University of Brescia. ERGO - Fluid Test Laboratory, 2024. https://ergo.unibs.it/.
[29] K.R. Hall, P.T. Eubank, A.S. Myerson, W.E. Nixon, A new technique for collecting binary vapor-liquid equilibrium data without measuring composition: the method of intersecting isochores, AIChE J 21 (1975) 1111–1114, https://doi.org/10.1002/aic.690210610.
[30] E.S. Burnett, Compressibility determinations without volume measurements, J. Appl. Mech. 3 (2021) A136–A140, https://doi.org/10.1115/1.4008721.
[31] C.E. Stouffer, S.J. Kellerman, K.R. Hall, J.C. Holste, B.E. Gammon, K.N. Marsh, Densities of carbon dioxide + hydrogen sulfide mixtures from 220 K to 450 K at pressures up to 25 MPa, J. Chem. Eng. Data. 46 (2001) 1309–1318, https://doi.org/10.1021/je000182c.
[32] J. Zhou, P. Patil, S. Ejaz, M. Atilhan, J.C. Holste, K.R. Hall, Vm, T) and phase equilibrium measurements for a natural gas-like mixture using an automated isochoric apparatus, J. Chem. Thermodyn. 38 (2006) 1489–1494, https://doi.org/10.1016/j.jct.2005.12.011.
[33] J. Zhou, K.R. Hall, J.C. Holste, Automated isochoric apparatus for pVT and phase equilibrium studies of natural gas mixtures, in: AIChE Annu. Meet. Conf. Proc, 2004, pp. 3477–3480.
[34] A. Velez, P. Hegel, G. Mabe, E.A. Brignole, Density and conversion in biodiesel production with supercritical methanol, Ind. Eng. Chem. Res. 49 (2010) 7666–7670, https://doi.org/10.1021/ie100670r.
[35] M.U. Goni, R. Burgass, A. Chapoy, P. Ahmadi, Isochoric bubble point data for binary systems of 1 (ethane) in 2 (decane, undecane, dodecane and tridecane), Fluid Phase Equilib 577 (2024) 113968, https://doi.org/10.1016/j.fluid.2023.113968.
[36] Sol Group, (n.d.). https://www.sol.it/it (accessed February 28, 2024).
[37] ThermoFisher Scientific (ex Alfa Aesar), (n.d.). https://www.thermofisher.com/it/en/home.html (accessed February 28, 2024).
[38] Sigma Aldrich, (n.d.). https://www.sigmaaldrich.com/IT/it (accessed February 28, 2024).
[39] abcr GmbH, (n.d.). https://abcr.com/(accessed February 28, 2024).
[40] E. Neyrolles, A. Valtz, C. Coquelet, A. Chapoy, On the phase behaviour of the CO2 + N2O4 system at low temperatures, Chem. Eng. Sci. 258 (2022) 117726, https://doi.org/10.1016/j.ces.2022.117726.
[41] C. Coquelet, A. Valtz, P. Théveneau, Experimental determination of thermophysical properties of working fluids for ORC applications, in: 2019. https://doi.org/10.5772/intechopen.87113.
[42] D.Y. Peng, D.B. Robinson, A new two-constant equation of state, Ind. Eng. Chem. Fundam. 15 (1976) 59–64, https://doi.org/10.1021/i160057a011.
[43] H.I. Britt, R.H. Luecke, The estimation of parameters in nonlinear, implicit models, Technometrics 15 (1973) 233–247, https://doi.org/10.1080/00401706.1973.10489037.
[44] W.E. Deming, Statistical Adjustment of Data, Dover Publication Inc., New York, 1943.
[45] Aspen Plus®, Version V12.1, Aspen Technology Inc, 2022.
[46] H. Cheng, M.E. Pozo De Fernández, J.A. Zollweg, W.B. Streett, Vapor-liquid equilibrium in the system carbon dioxide + n-Pentane from 252 to 458 K at Pressures to 10 MPa, J. Chem. Eng. Data. 34 (1989) 319–323, https://doi.org/10.1021/je00057a018.
[47] G.J. Besserer, D.B. Robinson, Equilibrium-phase properties of n-pentane-carbon dioxide system, J. Chem. Eng. Data. 18 (1973) 416–419, https://doi.org/10.1021/je60059a020.
[48] F.H. Poettmann, D.L.V. Katz, Phase behavior of binary carbon dioxide-paraffin systems, Ind. \& Eng. Chem 37 (1945) 847–853. https://api.semanticscholar.org/CorpusID:98720285.
[49] [Ruhr-U.B. (Germany)]" O, R. Kunz, W. Klimeck, M.[E.O.R.A.G. Wagner, Jaeschke Dorsten (Germany)]," The GERG-2004 Wide-Range Equation of State For Natural Gases and Other Mixtures, VDI-Verlag, Duesseldorf (Germany), Germany, 2007.
[50] E.W. Lemmon, Ian H. Bell, M.L. Huber, M.O. McLinden, NIST standard reference database 23: reference fluid thermodynamic and transport properties-REFPROP, version 10.0, Natl Inst. Stand. Technol. (2018), https://doi.org/10.18434/T4/1502528.
[51] P. Ganesan, T.M. Eikevik, New zeotropic CO2-based refrigerant mixtures for cascade high-temperature heat pump to reach heat sink temperature up to 180°C, Energy Convers. Manag. X. 20 (2023), https://doi.org/10.1016/j.ecmx.2023.100407.
[52] J.F. Boston, P. Mathias, Phase equilibria in a third-generation process simulator, EFCE Publ. Ser. (European Fed. Chem. Eng. (1980) 823–849.
[53] D.S.H. Wong, S.I. Sandler, A theoretically correct mixing rule for cubic equations of state, AIChE J 38 (1992) 671–680, https://doi.org/10.1002/aic.690380505.
[54] G. Soave, Equilibrium constants from a modified Redlich-Kwong equation of state, Chem. Eng. Sci. 27 (1972) 1197–1203, https://doi.org/10.1016/0009-2509(72)80096-4.